TOOLS AND TECHNIQUES

Analysis of Sealing Mechanical Properties of Fracturing Packer Under Complex Conditions

Zhaoyi Liu (ID) · **Shibin Li** · **Ligang Zhang** · **Fengshan Wang** ·
Peng Wang · **Lingling Han** · **Yuanyuan Ma** · **Haijun Zhang**

Abstract As the core component of the fracturing tool, the packer cartridge plays a vital role in a horizontal well stimulation and transformation process (Sun and Bai in Pet Explor Dev 44:1022–1029, 2017). Influenced by many factors such as formation workflow, borehole structure and construction conditions, the mechanical response of the packer rubber cylinder in sealing is complex and changeable (Jun et al. in J Pet Sci Eng 171:495–506, 2018; Tong et al. J Pet Sci Eng 172:964–975, 2019; Zhu et al. J Pet Sci Eng 151:311–317, 2017b). In order to study the mechanical response mechanism of the packer tool under complex working conditions, tensile tests of rubber under the corrosion environment of carbon dioxide formation fluid were carried out and the constitutive material parameters of *Yeoh* model after corrosion were obtained. The results showed that the tensile strength of hydrogenated nitrile butadiene rubber (HNBR) decreased by 7.86–17.01% after corrosion in simulated formation fluid, and the elongation at break increased by 2.09–19.74%. Compared with AFLAS (tetrapropyl fluoro elastomer), HNBR rubber had better stability and can be used as the preferred material for the service environment of permanent packers. Based on the mechanical properties of numerical calculation results before and after corrosion, it was found that the contact pressure and compression distance of the whole HNBR packer changed slightly, which met the requirements of field construction. On the basis of optimum selection of rubber material, the sealing performance of packer in borehole casing with enlargement/reduction caused by formation is analyzed. The results show that the casing with expansion deformation will lead to setting lag or lax, and the shrinkage casing will lead to setting advance or even stress failure. The analysis results provide theoretical support for the improvement in permanent packer string and its adaptation to complex formation.

Keywords Permanent packer · Rubber cylinder · Corrosion · Casing deformation

Z. Liu (✉) · S. Li · L. Zhang · Y. Ma
Department of Petroleum Engineering, Northeast Petroleum University, Daqing 163318, China
e-mail: tim0272@163.com

F. Wang · P. Wang
Production Engineering and Research Institute, Daqing Oilfield, Daqing 163453, China

L. Han
The Research Institute of Petroleum Exploration and Development-LangFang, Langfang 065007, China

H. Zhang
Institute of Petroleum Engineering, Dagang Oilfield, Tianjin 300280, China

Introduction

The packer is an elastic sealing element between the casing and the oil pipe, which is used to seal the annular space [1, 2]. There are many types of packers, among which the permanent packer is mainly used in oil and gas well fracturing, completion, acidification, oil testing and other downhole operations [3]. The quality of the packer [4] plays a decisive role in the packer's sealing effect and service life. The good working performance of the packer depends not only on its structural design, but also on its material characteristics and working environment [5]. For example, thinning of a worn casing inner wall, buckling of the casing in large displacement horizontal sections and corrosion of formation water containing acidic carbon dioxide will reduce the working

1570

J Fail. Anal. and Preven. (2019) 19:1569–1582

reliability of packer rubber cylinder [6–8]. The failure of the rubber cylinder is mainly caused by high temperature, high pressure and corrosion in underground, of which the main manifestations are aging of rubber, tearing of the rubber cylinder and release of elastic contact stress between the rubber cylinder and the casing inner wall. The research progress of permanent packers in China is fast, and the temperature and pressure resistance index basically meet the domestic demand of conventional oil and gas wells. However, there are still many problems to be solved in the material and structure design optimization for high temperature and high pressure deep oil and gas reservoirs. At present, HNBR (hydrogenated nitrile butadiene rubber) and AFLAS (tetrapropyl fluoro elastomer) rubbers are the main materials used in packers of deep gas reservoirs in the Daqing Oilfield. By comparing the tensile strength and elongation at break of two kinds of rubber before and after corrosion in simulated formation fluid, and calculating the overall sealing performance of rubber cylinders before and after corrosion, a theoretical basis is provided for the selection of rubber materials for packers. On this basis, the mechanical response of a rubber cylinder under different wellbore deformation conditions was analyzed, which provided technical guidance for later structural optimization design and field construction.

Permanent Packer Structure

The structure of a permanent packer is mainly composed of an upper joint, sealing section, working cylinder, central pipe, upper slip, rubber tube, lower slip, lock ring, jacket and lower joint, of which the component of rubber tube is made up of HNBR/AFLAS, as shown in Fig. 1.

Performance Test Before and After Corrosion

Test Conditions

Segmental fracturing of horizontal wells is a key technology for the development of deep gas reservoirs in Daqing,

which is of great significance to effectively improve productivity and reduce the seepage resistance of natural gas in formation. The key to fracturing technology in horizontal wells is the application of fracturing matching tools, in which the packer element plays an important role. However, high burial depth, high pressure and high acid corrosion gas content of tight gas reservoirs require higher performance and life of fracturing packer tools. Based on the present situations, it is of great significance to optimize and transform the imported integrated well completion fracturing string (permanent packer).

The simulated formation water for the corrosion test included the data of CO_2 content and formation water. The content of CO_2 was 3.55%, the content of Cl^- in simulated formation water was 7500 mg/L, and the test was in simulated formation water for 24 h.

Sample Preparation

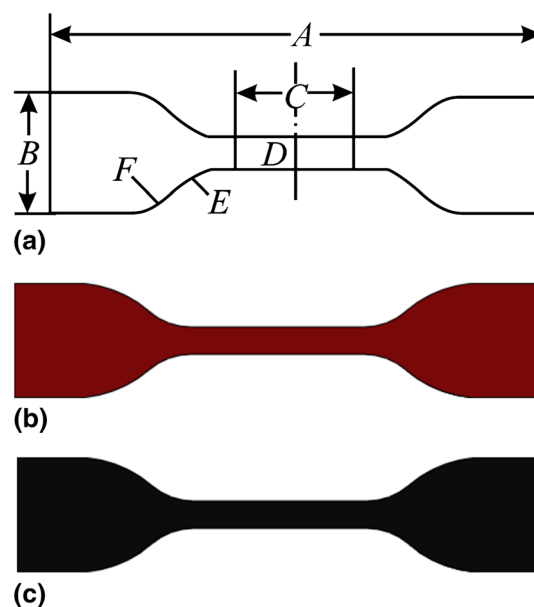In this paper, two different kinds of rubber materials, HNBR and AFLAS, were tested under the condition of

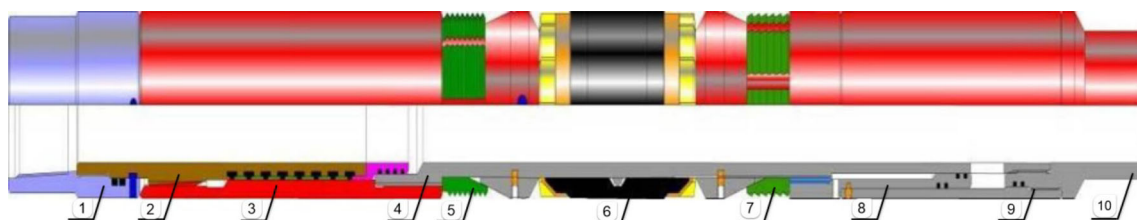**Fig. 2** Dumbbell-shaped rubber tensile specimens

Fig. 1 Permanent packer structure: 1. upper joint, 2. seal section, 3. working cylinder, 4. central tube, 5. upper slip, 6 rubber cylinder (barrel), 7. lower slip, 8. lock ring, 9. tube coat and 10. down connector

simulated formation water. The properties of the rubbers before and after corrosion were compared and analyzed. According to (GB/T1701-2001; GB/T528, 2009; GB/T533,

Fig. 3 Electronic universal material testing machine

2008), the dumbbell uniaxial tensile test (Figs. 2 and 3) was carried out, the test speed was 500 mm/min, and the hyperelastic constitutive models of the two rubber materials before and after corrosion were obtained. The black specimens were HNBR, unsoaked samples (A, B, C) and soaked samples (D, E, F) in simulated formation water; the red specimens were AFLAS rubber, unsoaked samples (G, H, I) and soaked samples (J, K, L) in simulated formation water. The sample dimensions are shown in Table 1.

Tensile Test Results Before and After Corrosion

Uniaxial Stretching Data Results

The deformation detected by the test equipment is the deformation amount of the two working marking lines, and the tensile force–deformation displacement curve is drawn as in Fig. 4.

Uniaxial Stretching Data Processing

For dumbbell-shaped rubber specimens, according to GB/T528 and GB/T533 (GB/T528, 2009; GB/T533, 2008), the tensile strength TS was calculated according to formula (1) and expressed in MPa:

$$TS = \frac{F_m}{DH} \tag{Eq 1}$$

The tensile strength at break TS_b was calculated according to formula (2) and expressed in MPa:

Table 1 Dimensional parameters of dumbbell stretch rubber samples

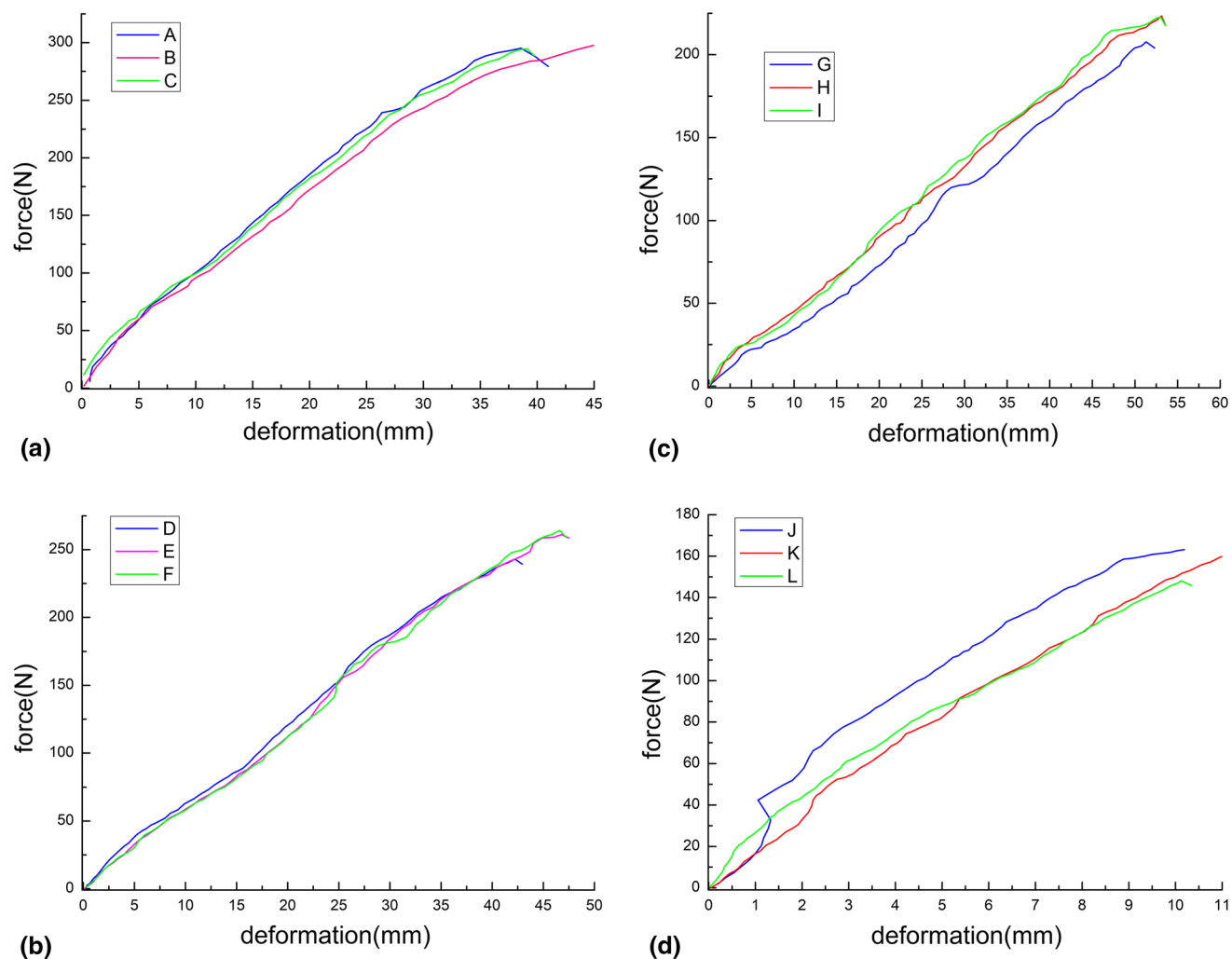| Sample number	Tip width (mm)	Work line distance (c/ mm)	Working part width (days/ mm)	Small radius (e/ mm)	Large radius (f/ mm)	Thickness (h/ mm)
Standard	25 ± 1.00	25 ± 1.00	6 ± 0.40	14 ± 1.00	25 ± 2.00	2 ± 0.20
A	25	25	6	14	25	3.40
B	25	25	6	14	25	3.41
C	25	25	6	14	25	3.42
D	25	25	6	14	25	3.35
E	25	25	6	14	25	3.31
F	25	25	6	14	25	3.35
G	25	25	6	14	25	3.36
H	25	25	6	14	25	3.36
I	25	25	6	14	25	3.32
J	25	25	6	14	25	3.20
K	25	25	6	14	25	3.35
L	25	25	6	14	25	3.18

Fig. 4 Uniaxial tensile force–deformation curves of the two kinds of rubber materials. (**a**) Tensile result curve of HNBR before corrosion, (**b**) tensile result curve of HNBR after corrosion, (**c**) tensile result curve of AFLAS before corrosion and (**d**) tensile result curve of AFLAS after corrosion

$$TS_b = \frac{F_b}{DH} \qquad (Eq\ 2)$$

The elongation at break Eb is calculated according to formula (3) and expressed in %:

$$E_b = \frac{100(A_b - A_0)}{A_0} \qquad (Eq\ 3)$$

where F_m—the maximum tensile force recorded, N; F_b—the force recorded at the time of the fracture, N; D—the width of the narrow portion of the cutter, mm; H—the thickness of the test length portion, mm; A_0—the original gage length of the test piece, mm; A_b—the gage length of the test piece at break, mm.

According to the results, the tensile strength of the two rubber materials decreased under the simulated working fluid environment, and the tensile strength reduction in HNBR rubber and AFLAS rubber was 7.86–17.01 and 19.53–30.31%, respectively (Figs. 5 and 6). After the corrosion tests, the elongation at break of AFLAS rubber decreased significantly, and the rate of decline was 69.34–80.96%. While the elongation at break of HNBR rubber increased slightly, and the rate of increase was 2.09–19.74%. It can be seen from the comprehensive comparison that the strength reduction in HNBR rubber under corrosive conditions was small, the elongation at break was slightly increased, and the overall performance was better. On the contrary, the tensile strength and tensile elongation at break of AFLAS rubber after the corrosion decreased sharply, and the molecular chains had been seriously damaged, which indicates an unacceptable material for the Daqing deep gas reservoir packer. Therefore, a numerical simulation study of a packer was carried out based on the parameters of HNBR rubber material after corrosion.
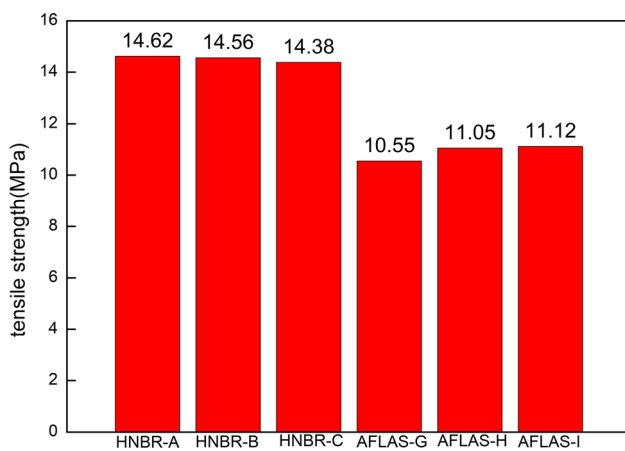
(a)
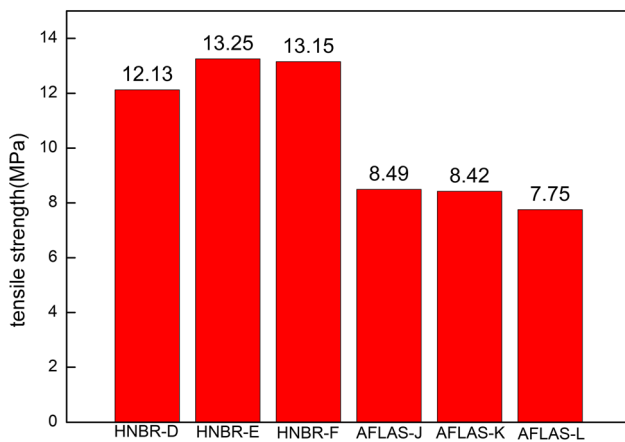
(b)

Fig. 5 Comparison of tensile strength before and after corrosion of two rubber materials. (**a**) Tensile strength before corrosion and (**b**) tensile strength after corrosion
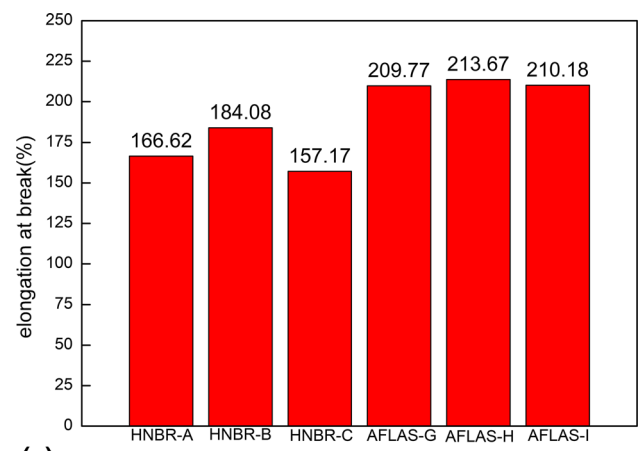

(a)

(b)

Fig. 6 Comparison of elongation at break before and after corrosion of two rubber materials. (**a**) Elongation at break before corrosion and (**b**) elongation at break before corrosion

Sealing Analysis of Permanent Packer Cylinder

Permanent Packer Cartridge Structure Model

According to the working principle of the permanent packer cartridge, the rest of the packer was ignored in the calculation model, because the inner tube has little effect on the cylinder calculation, and it was simplified into a solid cylinder, a sleeve and a gasket; the center tube was steel, the protection ring was made of copper, and the barrel was HNBR rubber. The simplified finite element model and meshing cross-sectional results are shown in Fig. 7.

Rubber Hyperelastic Constitutive Model

Compared with other solids, rubber materials are easily deformed and exhibit nonlinear viscoelastic properties as a whole. For the constitutive description of hyperelastic

materials, they are mainly divided into two categories, namely the phenomenological theoretical model and the network model of the statistical characteristics of molecular chains. Among them, the former studies the overall performance of rubber materials, while the latter focuses on the microscopic molecular chain structure and arrangement of rubber. This paper was carried out based on the former phenomenological theoretical model. At present, the more mature constitutive models at home and abroad mainly include the *Mooney–Rivlin* model (Mooney, 1940; Rivlin, 1948), the *Yeoh* model (Yeoh, 1993), *Gent* model (Gent, 1996) and the *Neo-Hooke* model (Ogden, 1997). Among them, the *Mooney–Rivlin* model can better fit the strain energy of the incompressible rubber material under moderate strain, but it is not suitable for compressing to large strains; the *Gent* model is mainly suitable for thin-walled spheres and thin-walled cylindrical tubular objects with internal pressure and is not suitable for strain energy under small-to-moderate strains; the *Yeoh* model [9, 10] can obtain constitutive parameters by uniaxial stretching,
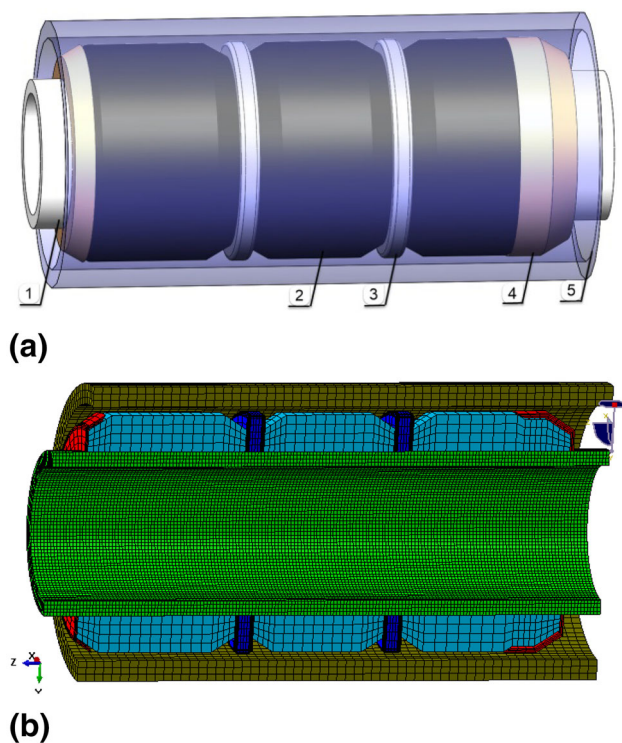
(a)

(b)

Fig. 7 Finite element model of permanent packer rubber cylinder: 1—central tube, 2—rubber tube, 3—gasket, 4—protective ring and 5—casing pipe

which agrees well with the experimental results under large deformation, but the simulation results are slightly worse under small deformation, and the *Gent* model is similar. The *Ogden* model can better reflect the entire deformation process, while the disadvantage is that many experiments are required to obtain parameters. Since the compression process of the rubber cylinder is a large deformation, and considering the problem of obtaining the experimental amount of the basic parameters, the *Yeoh* model was used in this paper and the coefficients C_{10}, C_{20} and C_{30} were obtained by the uniaxial tensile test to define the finite element of the permanent packer cylinder under different working conditions [3, 11].

For the constitutive relationship of the rubber material expressed by the strain energy density function, the relationship between the deformation tensor W ($I1$, $I2$, $I3$) and the main elongation ratio W ($\lambda 1$, $\lambda 2$, $\lambda 3$) is:

$$\left. \begin{array}{c} I_1 = \lambda_1^2 + \lambda_2^2 + \lambda_3^2 \\ I_2 = (\lambda_1\lambda_2)^2 + (\lambda_2\lambda_3)^2 + (\lambda_3\lambda_1)^2 \\ I_3 = (\lambda_1\lambda_2\lambda_3)^2 \end{array} \right\} \tag{Eq 4}$$

For absolutely incompressible materials, then

$$I_3 = (\lambda_1\lambda_2\lambda_3)^2 = 1 \tag{Eq 5}$$

$$\lambda_3 = \frac{1}{\lambda_1\lambda_2} \tag{Eq 6}$$

$$\left. \begin{array}{c} I_1 = \lambda_1^2 + \lambda_2^2 + \frac{1}{\lambda_1^2\lambda_2^2} \\ I_2 = (\lambda_1\lambda_2)^2 + \frac{1}{\lambda_1^2} + \frac{1}{\lambda_2^2} \end{array} \right\} \tag{Eq 7}$$

The expression of the main elongation ratio in the above formula is:

$$\lambda_i = 1 + \varepsilon_i \tag{Eq 8}$$

where ε_i—the strain in the direction of the main axis ($i = 1, 2, 3$).

The expression of the strain energy density function of the Yeoh model is:

$$W = \sum_{i=1}^{N} C_{i0}(I_1 - 3)^i + \sum_{i=1}^{N} \frac{1}{d_i}(J - 1)^{2i} \tag{Eq 9}$$

In the above formula, generally, N is set to 3 to achieve a better fitting effect, and J is set to 1 for incompressible material, then

$$\frac{\partial W}{\partial I_1} = C_{10} + 2C_{20}(I_1 - 3) + 3C_{30}(I_1 - 3)^2 \tag{Eq 10}$$

According to the mechanical derivation, the relationship between Kirchhoff stress tensor and Green strain tensor is obtained.

$$t^{ij} = \frac{\partial W}{\partial I_1}\frac{\partial I_1}{\partial \gamma_{ij}} + \frac{\partial W}{\partial I_2}\frac{\partial I_2}{\partial \gamma_{ij}} + \frac{\partial W}{\partial I_3}\frac{\partial I_3}{\partial \gamma_{ij}} \tag{Eq 11}$$

According to formulas (7) and (8), the relationship between principal stress and main elongation ratio can be derived:

$$\left. \begin{array}{c} t_1 = \frac{2}{\lambda_1}\left(\lambda_1^2 - \frac{1}{\lambda_1^2\lambda_2^2}\right)\left(\frac{\partial W}{\partial I_1} + \lambda_2^2\frac{\partial W}{\partial I_2}\right) \\ t_2 = \frac{2}{\lambda_2}\left(\lambda_2^2 - \frac{1}{\lambda_1^2\lambda_2^2}\right)\left(\frac{\partial W}{\partial I_1} + \lambda_1^2\frac{\partial W}{\partial I_2}\right) \end{array} \right\} \tag{Eq 12}$$

For uniaxial stretching, there is

$$\left. \begin{array}{c} t_2 = t_3 = 0 \\ \lambda_2^2 = \lambda_2^2 = \frac{1}{\lambda_1} \end{array} \right\} \tag{Eq 13}$$

Substituting Eq 13 into Eq 7, then

$$\left. \begin{array}{c} I_1 = \lambda_1^2 + \frac{2}{\lambda_1} \\ I_2 = 2\lambda_1 + \frac{1}{\lambda_1^2} \end{array} \right\} \tag{Eq 14}$$

Substituting Eq 13 into Eq 12, then

$$t_1 = 2\left(\lambda_1 - \frac{1}{\lambda_1^2}\right)\left(\frac{\partial W}{\partial I_1} + \frac{1}{\lambda_1}\frac{\partial W}{\partial I_2}\right) \tag{Eq 15}$$

Substituting Eq 10 into Eq 15, then

$$\frac{t_1}{2\left(\lambda_1 - \frac{1}{\lambda_1^2}\right)} = C_{10} + 2C_{20}\left(\lambda_1^2 + \frac{2}{\lambda_1} - 3\right)$$
$$+ 3C_{30}\left(\lambda_1^2 + \frac{2}{\lambda_1} - 3\right)^2 \qquad \text{(Eq 16)}$$
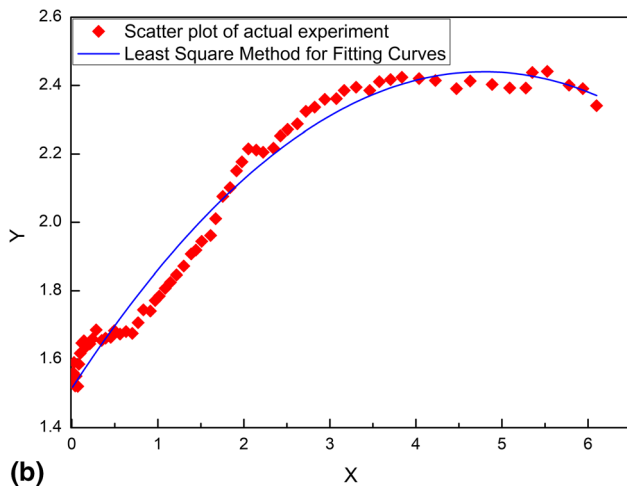
Let $\quad Y = \dfrac{t_1}{2\left(\lambda_1 - \frac{1}{\lambda_1^2}\right)}, \quad X = \left(\lambda_1^2 + \frac{2}{\lambda_1} - 3\right), \quad$ then Eq 16

becomes as:

$$Y = C_{10} + 2C_{20}X + 3C_{30}X^2 \qquad \text{(Eq 17)}$$

The HNBR rubber in the uniaxial tensile test results of the dumbbell-shaped rubber was subjected to data processing before and after corrosion (Fig. 8), and the constitutive parameters of the *Yeoh* model are obtained as shown in Table 2.
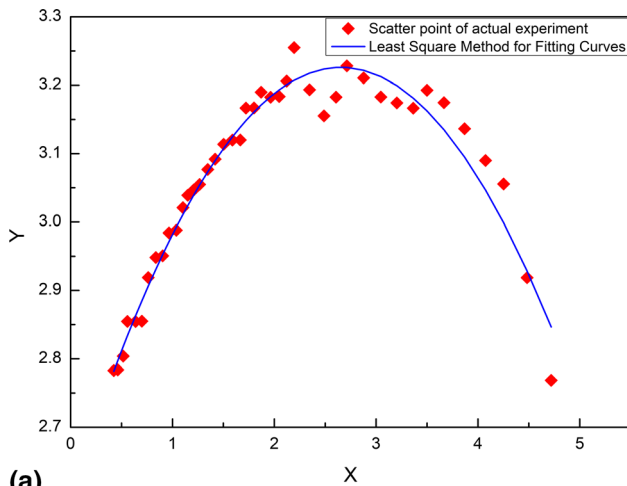
Fig. 8 Data extraction and Yeoh relationship fitting before and after HNBR rubber corrosion. (**a**) Parameter fitting curve before corrosion and (**b**) parameter fitting curve after corrosion

Table 2 Results of Yeoh constitutive parameters for HNBR rubber tests before and after corrosion

Test conditions	C_{10}	C_{20}	C_{30}
Before corrosion	− 0.02973	0.2369	2.5970
After corrosion	− 0.01347	0.1934	1.5144

Boundary Conditions and Parameter Settings

According to the actual work of the permanent packer, during the setting process, the slip at the one end of the packer will no longer produce displacement after anchoring, and fixed constraints will be set; at the other end, the rubber tube was squeezed by the cone and expands and deforms until the end of seating, when the packer rubber cylinder completely seals the outer side of the tubing and the inner wall of the casing. Detailed boundary settings are shown below.

(1) Fixed constraints were set on the outer surface of the casing and on both ends of the central pipe;
(2) The upper protective ring was subjected to axial load of 10 MPa;
(3) Face-to-face contact was set between adjacent parts, the friction coefficient between metals was set to 0.1, and the friction coefficient between rubber and metal was set to 0.3, while that between rubbers was 0.47.
(4) Casing damage and deformation occurred in some casing during construction, and the effect of casing size change on sealing was considered.

Simulation Results Analysis

By comparing and analyzing the sealability of the rubber cylinder before and after the formation fluid corrosion, it can be seen from Figs. 9, 10, 11 and 12 that the performance of the HNBR rubber cylinder does not decline significantly, and it had good adaptability in the deep formation fluid, which can meet the actual construction needs. In addition, the contact stress and deformation between the rubber cylinder and compression ring were large, so optimizing the chamfer of the rubber cylinder and optimizing the material of the compression ring were of great significance for protecting the rubber cylinder. In the process of the rubber cylinder being compressed, the maximum compression deformation occured at the side of the rubber cylinder, and its stress and sealing were the most important in the whole working system, which was the key to improve the adaptability in the later harsh environment.
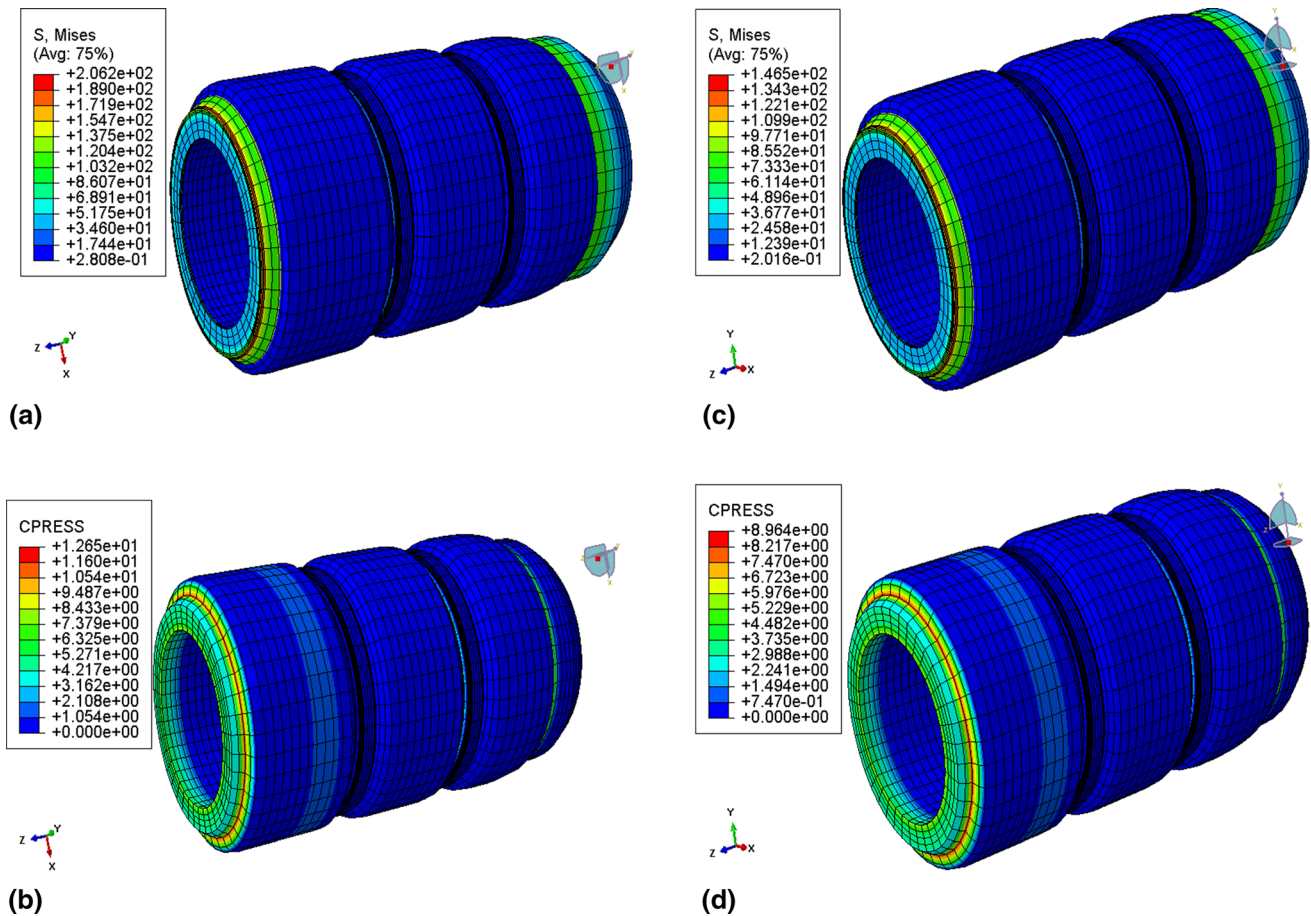
Fig. 9 Contact force numerical results of HNBR packer under axial loading of 10 MPa. (a) Contact stress of packer before corrosion, (b) contact pressure of packer before corrosion, (c) contact stress of packer after corrosion and (d) contact pressure of packer after corrosion

Sealing Result Processing

The stress of a single rubber cylinder before and after corrosion of HNBR rubber cylinder was extracted, and the deformation maps at different compression times were drawn, respectively. The contact stress maps are shown in Figs. 13 and 14.

According to the data, it can be concluded that when the outer contour surface of the rubber drum was compressed and expanded to a certain extent, it was close to the inner wall of the casing, and there will be no deformation in the radial direction after sealing. In addition, during the compression process, the radial deformation rate was faster in the early stage and gradually decreased from the late stage of compression to the complete closure of the inner wall of the casing until it was completely sealed. After sealing, the contact force between the rubber cylinder and the inner wall of the casing became an arch bridge (small on both sides and large in the middle), and the force of the three rubber cylinders decreased in turn. The deformation of the initial compressed rubber cylinder was the most significant, which was also the key of sealing pressure, significantly affecting the working life of the packer.

Effect of Casing Clearance on Packer Sealing

According to the performance parameters of corroded HNBR rubber cylinder, the whole setting process was analyzed, and the relationship curves between the compression distance of the rubber cylinder and the contact stress of the rubber cylinder varying with the axial load are drawn as in Fig. 15.

Fig. 10 Numerical results of deformation of rubber cylinder before and after corrosion. (**a**) X-direction deformation of packer before corrosion and (**b**) X-direction deformation of packer after corrosion
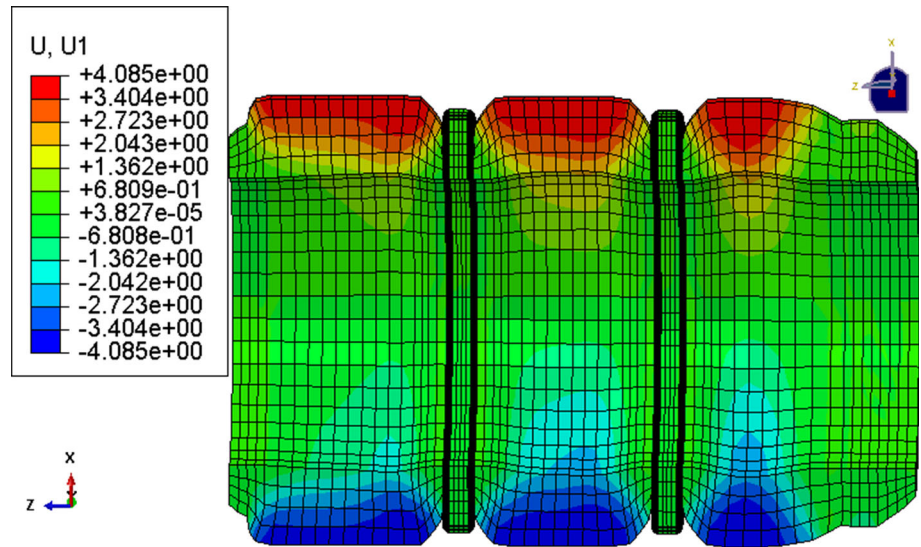
(a)
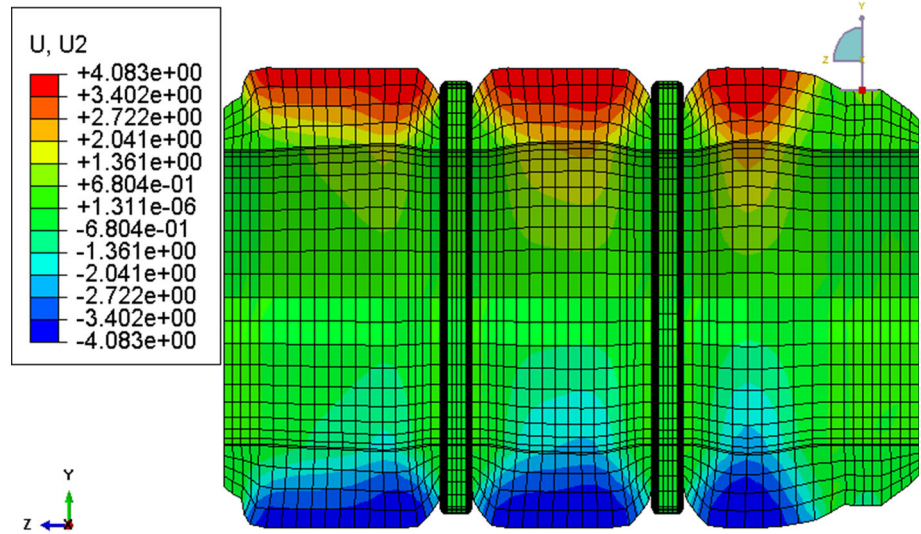
(b)

According to the setting result, the cylinder liner pushed the cone to produce axial load, and the side rubber cylinder was compressed. In the initial state, with the increase in axial load, the rubber cylinder was compressed and the compression distance increased sharply. When the axial load reached 5 MPa, the rubber cylinder came into contact with the casing and contact force developed between the casing and packer. With the axial load continuing to increase to 15 MPa, the growth rate of compression distance gradually decreased, the contact force and effective contact area of the casing rapidly increased, and then complete seating occurred. As the axial load continued to
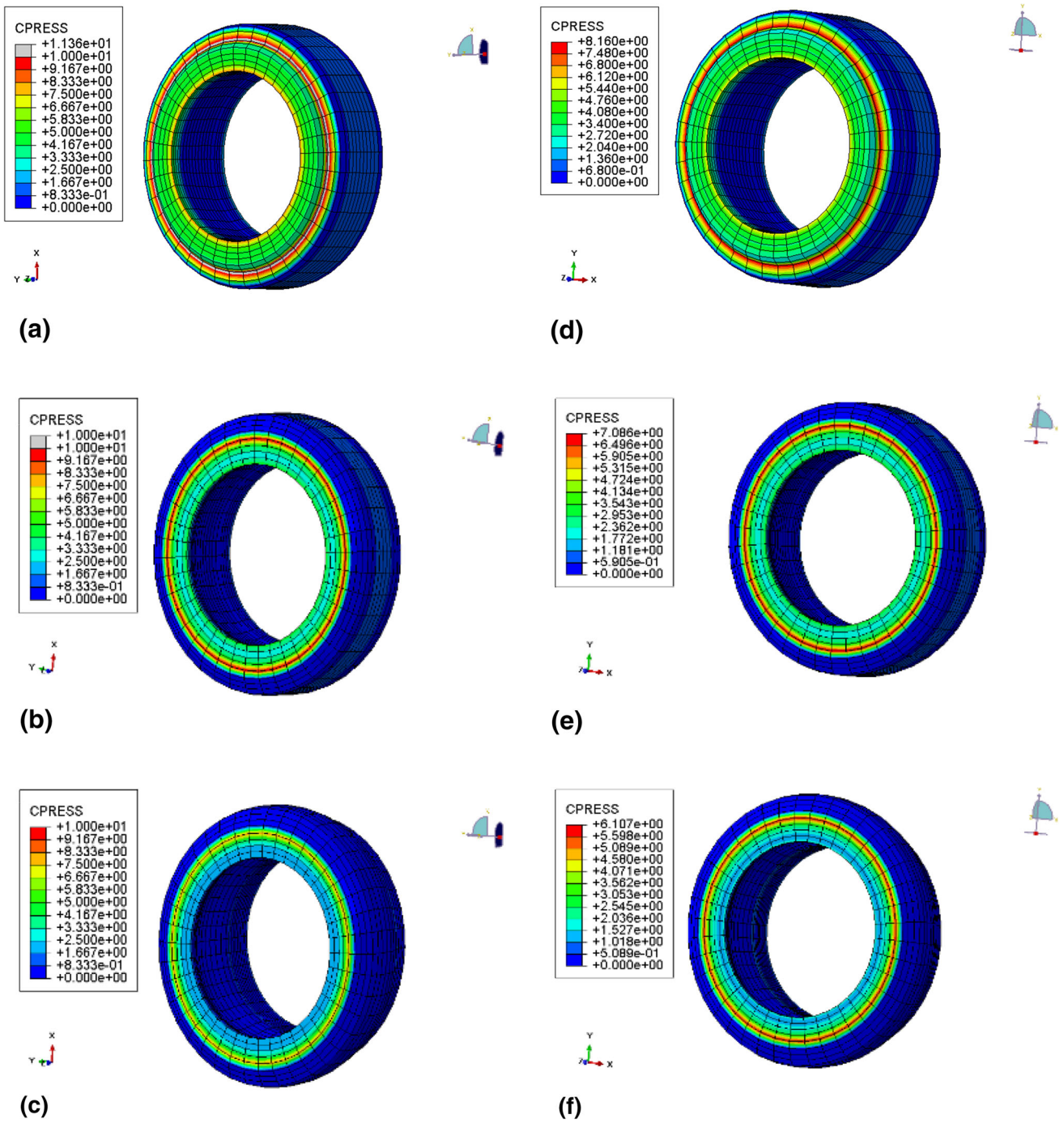
Fig. 11 Numerical results of contact force of rubber cylinders before and after corrosion. (**a**) Rubber cylinder 1 before corrosion, (**b**) rubber cylinder 2 before corrosion, (**c**) rubber cylinder 3 before corrosion, (**d**) rubber cylinder 1 after corrosion, (**e**) rubber cylinder 2 after corrosion and (**f**) rubber cylinder 3 after corrosion
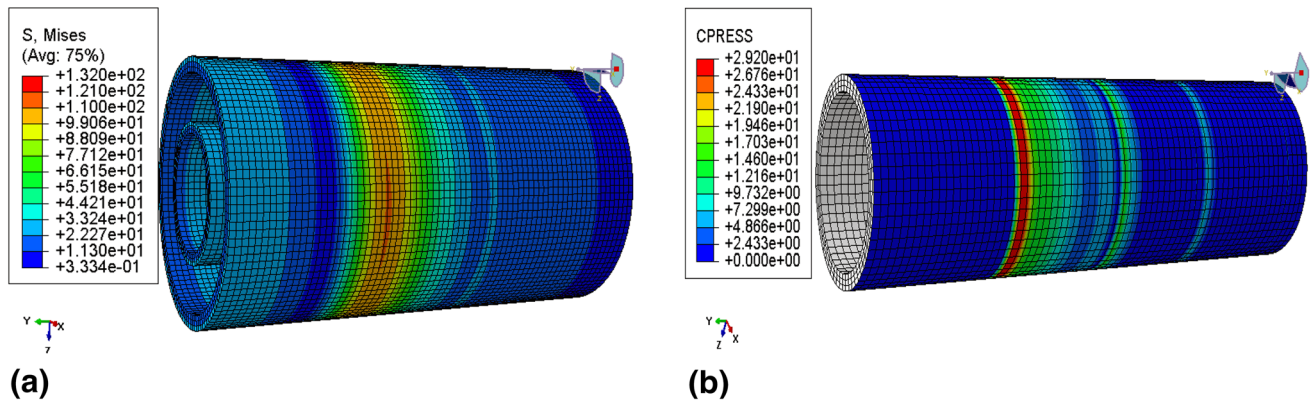
Fig. 12 Contact force between inner and outer sides of rubber cylinder between pipe strings. (**a**) Casing contact stress and (**b**) contact pressure of central pipe

increase, the compression distance will not change; however, the contact pressure continued to increase, because the rubber cylinder had filled the whole tubing and casing annular space with axial compression and radial expansion, but the volume of the rubber cylinder did not change any more in this time, when the whole packer rubber cylinder was completely seated (Fig. 16).

Effect of Casing Clearance on Packer Sealing

In the actual fracturing process, fracturing fluid could cause some casing deformation [12], which will lead to large casing expansion or shrinkage [13–15], so casing sealing analysis under different clearances was carried out, and the sealing adaptability of the packer was evaluated according to the results [16–18]. It is of great engineering significance to study packer performance systematically and comprehensively for staged fracturing and EOR of horizontal wells in tight gas reservoir [19–22]. In this paper, the difference of the maximum diameter between the inner wall of the casing and the initial rubber drum was set as D (mm). In field construction, the inner diameter of the casing was 121 mm, and the outer diameter of the rubber cylinder was 113 mm, then $D = 8$ mm, and (± 2 mm) was set as the object of analysis.

According to the calculation results, with the increase in casing clearance, the compression distance of the rubber cylinder increases and the contact stress decreased under the same axial load. In addition, after casing expansion, the packer exhibited a setting lag phenomenon, and its sealing performance will be reduced correspondingly; and even the result of sealing failure could occur when the casing was squeezed by formation pressure to shrink its diameter, and the packer exhibited advanced sealing phenomenon. Under the same axial load, the sealing pressure was larger, and under the larger setting load, the rubber cylinder would reach the stress limit and cause strength damage, even seal failure.

Conclusion

(1) By analyzing the mechanical properties of two kinds of rubber material specimens immersed in simulated corrosive solution, the rubber barrel material suitable for completion fracturing integral string of deep gas reservoir in Daqing was preliminarily optimized.

(2) Nonlinear finite element method was used to analyze the sealing process of rubber cylinders of permanent packer, and the results of contact stress and deformation were obtained. It is instructive for precise analysis of the sealing state and stress distribution of the rubber cylinder.

(3) The numerical study of casing shrinkage and enlargement in conventional fracturing process shows that shrinkage of the casing can cause packer setting and stress damage in advance, and casing expansion can cause packer setting lag or even improper sealing, which has technical guiding significance for large-scale fracturing construction in the future.
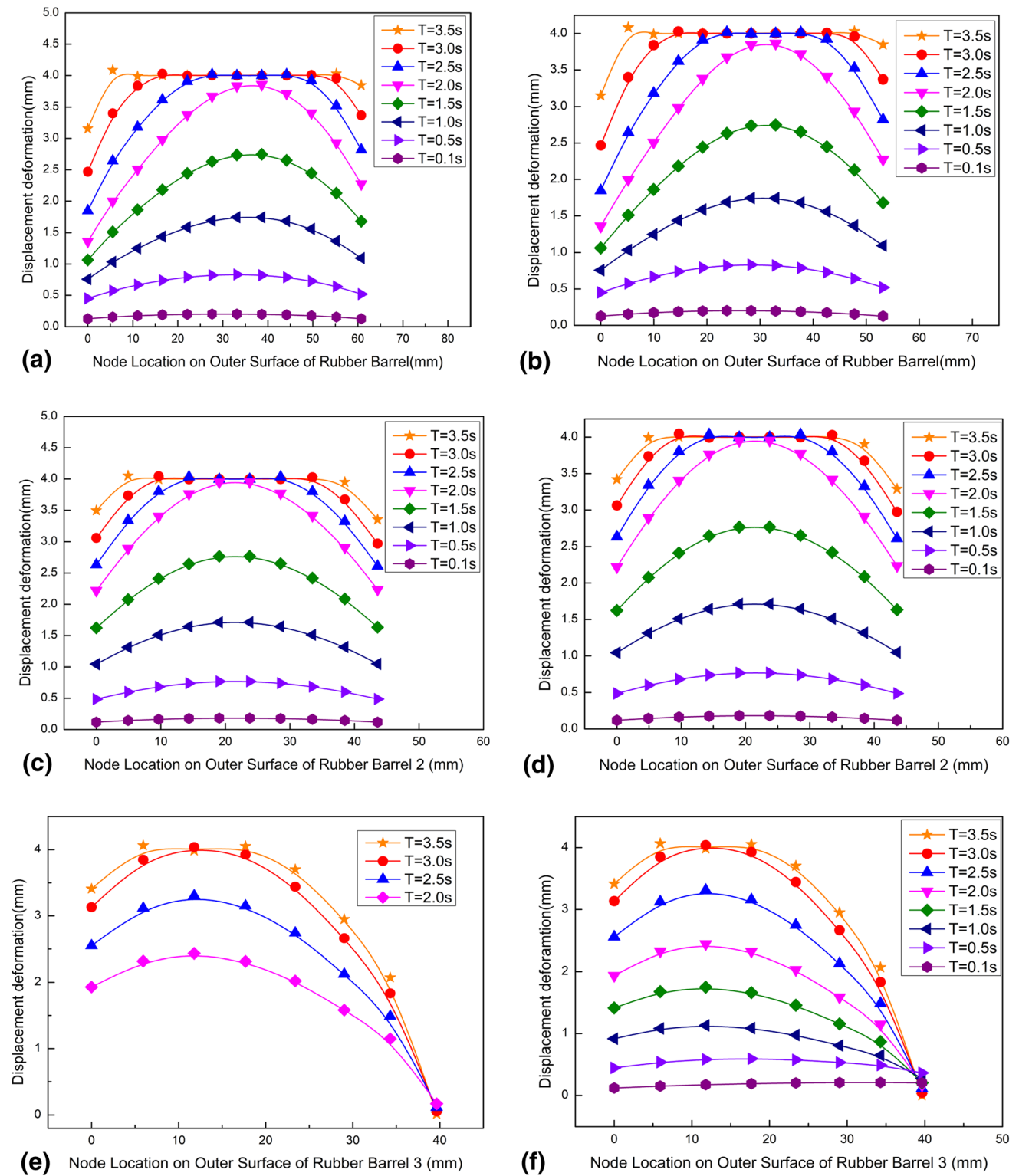
1580

J Fail. Anal. and Preven. (2019) 19:1569–1582

Fig. 13 Compression deformation curve of HNBR rubber barrel before and after corrosion. (**a**) Compression deformation of upper rubber barrel before corrosion and (**b**) compression deformation of upper rubber barrel after corrosion (**c**) compression deformation of middle rubber barrel after corrosion (**d**) compression deformation of middle rubber barrel after corrosion (**e**) compression deformation of down rubber barrel after corrosion (**f**) compression deformation of down rubber barrel after corrosion
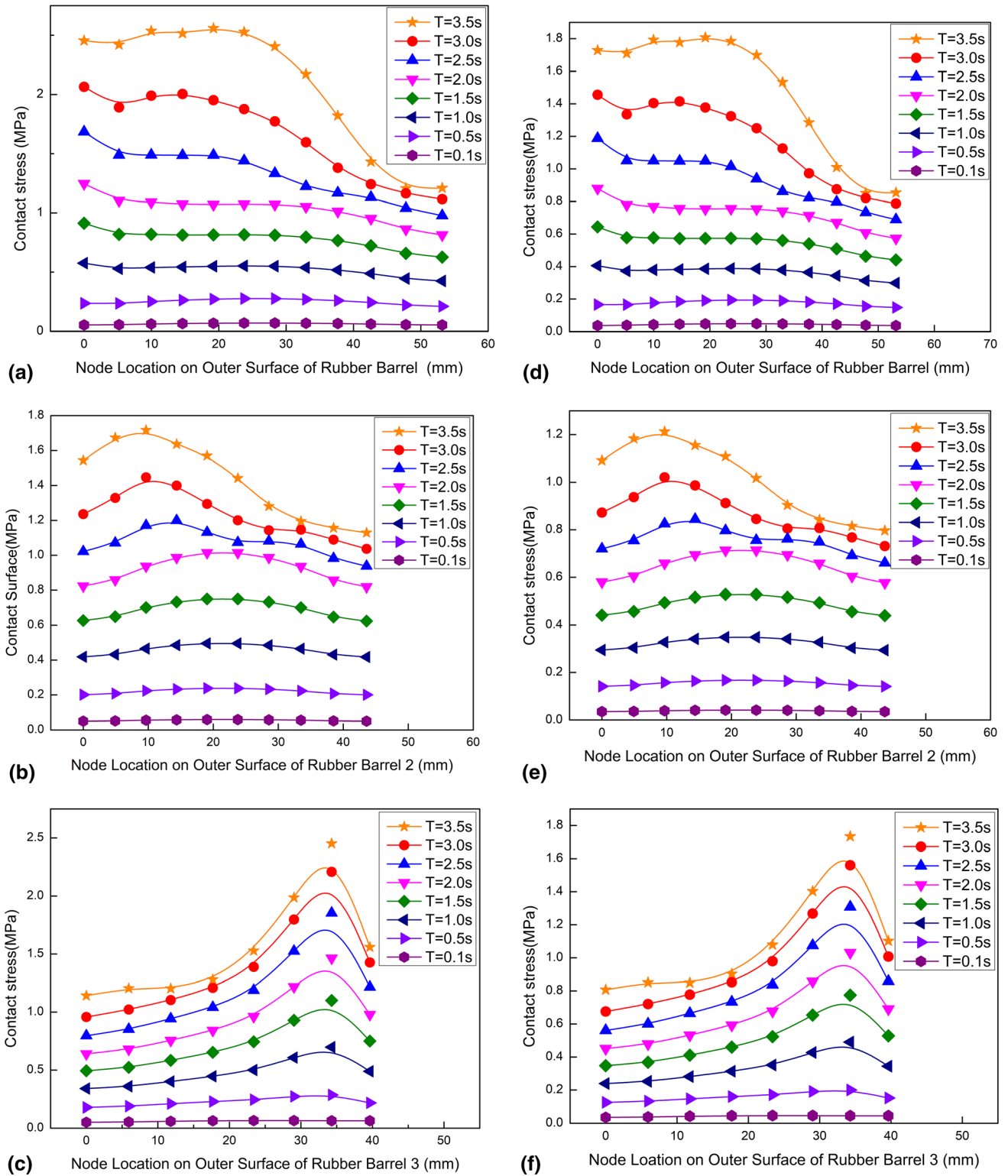
Fig. 14 Contact contact stress curve of HNBR rubber cylinder before and after corrosion. (**a**) Contact stress of upper rubber barrel before corrosion and (**b**) contact stress of middle rubber barrel before corrosion and (**c**) contact stress of down rubber barrel before corrosion and (**d**) contact stress of upper rubber barrel after corrosion and (**e**) contact stress of middle rubber barrel after corrosion and (**f**) contact stress of upper rubber barrel after corrosion
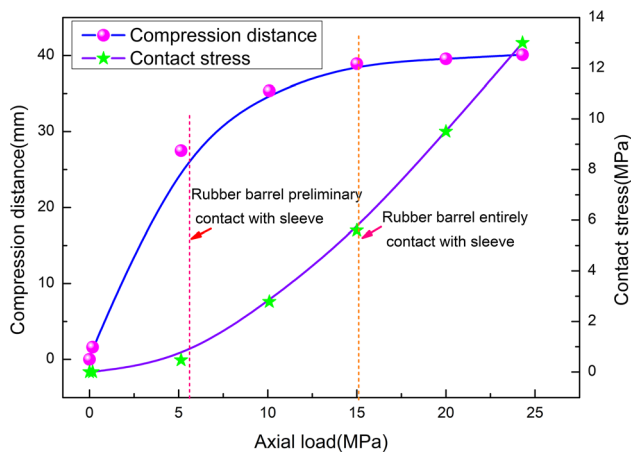
1582

J Fail. Anal. and Preven. (2019) 19:1569–1582

Fig. 15 Sealing result curve of HNBR rubber cylinder after corrosion
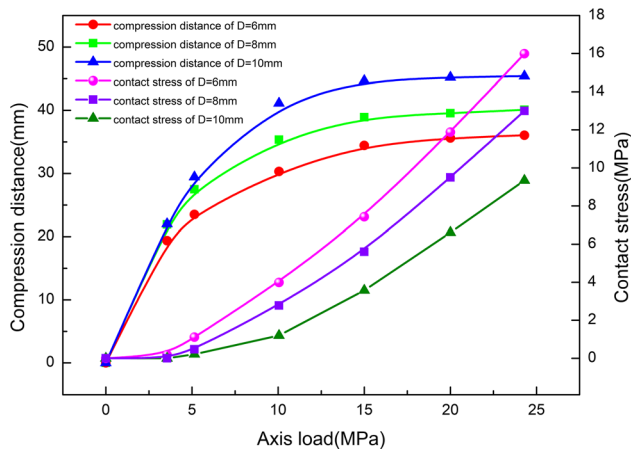
Fig. 16 Sealing result of packer affected by casing clearance

Conflict of interest The authors have no conflict of interest to report.

References

1. S.A. Al-Hiddabi, T. Pervez, S.Z. Qamar, F.K. Al-Jahwari, F. Marketz, S. Al-Houqani, M. van de Velden, Analytical model of elastomer seal performance in oil wells. Appl. Math. Model. **39**, 2836–2848 (2015)
2. Y.-F. Chen, M.-M. Liu, S.-H. Hu, C.-B. Zhou, Non-Darcy's law-based analytical models for data interpretation of high-pressure packer tests in fractured rocks. Eng. Geol. **199**, 91–106 (2015)
3. G. Hu, P. Zhang, G. Wang, M. Zhang, M. Li, The influence of rubber material on sealing performance of packing element in compression packer. J. Nat. Gas Sci. Eng. **38**, 120–138 (2017)
4. S.H.P. Cavalaro, A. Aguado, Packer behavior under simple and coupled stresses. Tunn. Undergr. Space Technol. **28**, 159–173 (2012)
5. D. Zhu, Y. Lin, H. Ma, H. Zhang, Y. Li, L. Zhang, K. Deng, Experimental studies on CO_2 corrosion of rubber materials for packer under compressive stress in gas wells. Eng. Fail. Anal. **80**, 11–23 (2017)
6. Y. Xi, J. Li, G. Liu, C. Cha, Y. Fu, Numerical investigation for different casing deformation reasons in Weiyuan-Changning shale gas field during multistage hydraulic fracturing. J. Pet. Sci. Eng. **163**, 691–702 (2018)
7. H. Yu, A.D. Taleghani, Z. Lian, Modelling casing wear at doglegs by incorporating alternate accumulative wear. J. Pet. Sci. Eng. **168**, 273–282 (2018)
8. X. Zhu, B. Liu, The reliability-based evaluation of casing collapsing strength and its application in marine gas reservoirs. Eng. Fail. Anal. **85**, 1–13 (2018)
9. O. Hesebeck, A. Wulf, Hyperelastic constitutive modeling with exponential decay and application to a viscoelastic adhesive. Int. J. Solids Struct. **141–142**, 60–72 (2018)
10. A. Karimi, M. Navidbakhsh, B. Beigzadeh, A visco-hyperelastic constitutive approach for modeling polyvinyl alcohol sponge. Tissue Cell **46**, 97–102 (2014)
11. X. He, X. Shi, M. Hoch, C. Gögelein, Mechanical properties of carbon black filled hydrogenated acrylonitrile butadiene rubber for packer compounds. Polym. Test. **53**, 257–266 (2016)
12. W. Yan, L. Zou, H. Li, J. Deng, H. Ge, H. Wang, Investigation of casing deformation during hydraulic fracturing in high geo-stress shale gas play. J. Pet. Sci. Eng. **150**, 22–29 (2017)
13. D.W.H. Su, Effects of longwall-induced stress and deformation on the stability and mechanical integrity of shale gas wells drilled through a longwall abutment pillar. Int. J. Min. Sci. Technol. **27**, 115–120 (2017)
14. F. Yin, Y. Deng, Y. He, D. Gao, B. Hou, Mechanical behavior of casing crossing slip formation in waterflooding oilfields. J. Pet. Sci. Eng. **167**, 796–802 (2018)
15. F. Yin, L. Han, S. Yang, Y. Deng, Y. He, X. Wu, Casing deformation from fracture slip in hydraulic fracturing. J. Pet. Sci. Eng. **166**, 235–241 (2018)
16. X. Li, C.S. El Mohtar, K.E. Gray, 3D poro-elasto-plastic modeling of breakouts in deviated wells. J. Pet. Sci. Eng. **174**, 913–920 (2019)
17. J. Wang, D. Kuanhai, Y. Zhiping, L. Bing, Y. Lin, Y. Feng, Study of technical specifications for non-API 140 casing in ultra-deep well. Eng. Fail. Anal. **97**, 115–127 (2019)
18. X. Zhu, B. Liu, A method to assess the reliability of casings in marine gas reservoirs based on Bayesian theory optimization. J. Pet. Sci. Eng. **172**, 1248–1256 (2019)
19. L. Jun, Z. Hongliang, L. Xian, L. Qingyou, X. Guohua, S. Xianming, Experimental study on the mechanical responses of downhole tools in highly-deviated waterflooding well. J. Pet. Sci. Eng. **171**, 495–506 (2018)
20. X. Sun, B. Bai, Comprehensive review of water shutoff methods for horizontal wells. Pet. Explor. Dev. **44**, 1022–1029 (2017)
21. Z. Tong, Q. Ye, J. Qian, Z. Hao, L. Wang, Down-hole isolation towards high-temperature reservoir using packing elements with swellable thermo-plastic vulcanizates. J. Pet. Sci. Eng. **172**, 964–975 (2019)
22. D. Zhu, Y. Lin, H. Zhang, Y. Li, D. Zeng, W. Liu, C. Qiang, K. Deng, Corrosion evaluation of packer rubber materials in CO_2 injection wells under supercritical conditions. J. Pet. Sci. Eng. **151**, 311–317 (2017)